

Helicity-conservative Physics-informed Neural Network Model for Navier-Stokes Equations

Ziqian Li, Jiwei Jia,** Young Ju Lee, Zheng Lu

April 18, 2022

Abstract

We design the helicity-conservative physics-informed neural network model for the Navier-Stokes equation in the ideal case. The key is to provide an appropriate PDE model as loss function so that its neural network solutions produce helicity conservation. Physics-informed neural network model is based on the strong form of PDE. We show that the relevant helicity-conservative finite element method based on the weak formulation of PDE can be somewhat different. More precisely, we compare the PINN formulation and the finite element method based on the weak formulation for conserving helicity and argue that for the conservation, strong PDE is more natural. Our result is justified by theory as well. Furthermore, a couple of numerical calculations are demonstrated to confirm our theoretical finding.

1 Introduction

Numerical simulation for the incompressible Navier-Stokes system is important in a number of applications. There have been a lot of efforts in designing stable and efficient numerical methods for solving the incompressible Navier-Stokes equations. The Navier-Stokes system has various conserved quantities. Among others, the energy law and the incompressibility ($\nabla \cdot \mathbf{u} = 0$) have been proved crucial. Particular, the helicity of a divergence-free vector field, which is conserved in non-dissipative systems (ideal flows), is a standard measure for the extent to which the field lines wrap and coil around one another [7]. Furthermore, fluid helicity is known to be important in the turbulence regime as discussed in, for example, [8, 26]. Helicity is also known to provide a local lower bound for the energy [3, p. 122], i.e., a topological obstruction of energy relaxation. We refer to [3, 4, 23, 24, 22] and the references therein for more discussions on fluids helicity. In many algorithms, these conservation laws are only approximated up to a discretization error, rather than exactly conserved. These approximation errors may then pollute the solution with unphysical behavior. It is therefore of great interest to construct numerical methods that precisely preserve the helicity. While it is very difficult to provide a complete review of the huge literature on incompressible Navier-Stokes simulations, we mention some existing efforts on helicity-preserving schemes. Liu and Wang [20] studied helicity-preserving finite difference methods for axisymmetric Navier-Stokes and MHD flows. Rebholz [18, 28] constructed energy- and helicity-preserving

**jiawei@jlu.edu.cn

finite element methods for the Navier-Stokes equations. See [25] for further discussions on, e.g., turbulence models. Kraus and Maj [15] studied helicity-preserving schemes for the MHD system based on discrete exterior calculus. See also [14] for helicity preserving schemes for MHD. To the best of our knowledge, however, it remains not attempted to use neural network models to preserve the helicity for the incompressible Navier-Stokes equation.

The goal of this paper is to construct the neural network model that can preserve the fluids helicity. Unlike the standard finite element methods based on the weak formulation of the PDE models, PINN model [27] is based on the strong PDE and thus, conservation can be shown to be made much easier without having to introduce a number of auxiliary variables. This is really the case for conserving the incompressibility. Later [19], [21] made great progress on deep learning solving PDEs and [13] discussed the theory of it. [16] proposed seq2seq strategy which is essential for timing problems. As is well-known the weak formulation seeks the pair of finite elements that is stable as well as is compatible such that the pressure space contains divergence of velocity so that the strong divergence is attained. However, such a construction is extremely difficult in general. Oftentimes, it relies on a discrete differential form point of view such as the finite element exterior calculus, see [9, 10] on structure-preserving discretization for the fluid mechanics with $H(\text{div})$ -conforming velocity. Recently, helicity has been discussed for the magnetic hydrodynamics equation. The flow equation is similar to similar discretization for the Navier-Stokes equations based on the Nédélec edge element can be found in [11]. However, helicity-preservation was not addressed there.

The rest of the paper is organized as follows. In Section 2, we provide preliminaries, notation and helicity-conservative finite element scheme. In Section 3, we present a PINN-based algorithm that preserves the helicity. In Section 4, we present numerical results on the convergence and helicity-preserving properties of our algorithms. In Section 5, we give some concluding remarks.

2 Governing Equation and Conservative Quantities

We consider the following system of equations in $\Omega \times (0, \mathbb{T}]$:

$$\partial_t \mathbf{u} - \mathbf{u} \times \boldsymbol{\omega} - R_e^{-1} \nabla \times \nabla \times \mathbf{u} + \nabla \left(\frac{1}{2} |\mathbf{u}|^2 + \tilde{p} \right) = \mathbf{f}, \quad (2.1a)$$

$$\boldsymbol{\omega} = \nabla \times \mathbf{u}, \quad (2.1b)$$

$$\nabla \cdot \mathbf{u} = 0. \quad (2.1c)$$

Here $\partial_t \mathbf{u} = \partial \mathbf{u} / \partial t$, \mathbf{u} and p are the fluid velocity and pressure, respectively. This formulation of the momentum equation (2.1a) is called the Lamb form [17].

We shall consider the following boundary conditions for (1): for all $x \in \partial\Omega$ and $t > 0$,

$$\mathbf{u} \times \mathbf{n} = \mathbf{0}, \quad p := \tilde{p} + \frac{1}{2} |\mathbf{u}|^2 = 0. \quad (2.2)$$

where \mathbf{n} is the unit outer normal vector. In fact, the conditions for \mathbf{u} and \tilde{p} in (2.2) can be seen as a vorticity boundary condition since $\mathbf{u} \times \mathbf{n} = \mathbf{0}$ implies $(\nabla \times \mathbf{u}) \cdot \mathbf{n} = 0$ on $\partial\Omega$. Girault [11] used similar conditions as (2.2) for the Navier-Stokes equations. As we shall see below, this is the natural boundary condition that appears in the helicity conservation.

The initial conditions for the fluid velocity, magnetic field are given for any $x \in \Omega$

$$\mathbf{u}(x, 0) = \mathbf{u}_0(x). \quad (2.3)$$

We now review some conserved quantities of (2.2) below. First, we can present the energy conservation without the proof (see [14] for example).

Theorem 1. *The diffusion or conservation of energy can be stated as follows. The NS system (2.1) with the boundary condition (2.2) has the following energy identity:*

$$\frac{1}{2} \frac{d}{dt} \|\mathbf{u}\|_0^2 + R_e^{-1} \|\nabla \times \mathbf{u}\|_0^2 = (\mathbf{f}, \mathbf{u}). \quad (2.4)$$

We note that the energy law (2.4) is important since it induces the energy norm stability:

$$\max_{0 \leq t \leq T} \|\mathbf{u}\|_0^2 + R_e^{-1} \int_0^T \|\nabla \times \mathbf{u}\|_0^2 d\tau \leq \|\mathbf{u}_0\|_0^2 + R_e \int_0^T \|\mathbf{f}\|_{-1}^2 d\tau.$$

Secondly, the main interest of this paper is the fluids helicity. We begin by defining the helicity

Definition 1. *For any divergence-free field ξ in Ω , the helicity of ξ is defined as*

$$\mathcal{H}_\xi := \int_\Omega \xi \cdot \eta \, dx, \quad (2.5)$$

where η is any potential of ξ satisfying $\nabla \times \eta = \xi$. By an integration by parts, \mathcal{H}_ξ does not depend on the choice of the potential η if $\xi \cdot \mathbf{n} = 0$ on the boundary $\partial\Omega$, c.f., [3].

We remark that the fluids helicity describes the linking and knots of the field ξ . In fluid mechanics, one defines the fluid helicity, denoted by \mathcal{H}_f as follows:

$$\mathcal{H}_f := \int_\Omega \mathbf{u} \cdot \nabla \times \mathbf{u} \, dx = \int_\Omega \mathbf{u} \cdot \boldsymbol{\omega} \, dx. \quad (2.6)$$

We state the precise form of helicity conservation as follows.

Theorem 2. *For the Euler equation, the following identity holds:*

$$\frac{d}{dt} \mathcal{H}_f = 2R_e^{-1} \int_\Omega \nabla \times \nabla \times \mathbf{u} \cdot \boldsymbol{\omega} \, dx + 2 \int_\Omega \mathbf{f} \cdot \boldsymbol{\omega} \, dx. \quad (2.7)$$

Proof. We notice that by the integration by parts together with the boundary condition for \mathbf{u} ,

$$\begin{aligned} \frac{d}{dt} \int_\Omega \mathbf{u} \cdot \boldsymbol{\omega} \, dx &= \int_\Omega \partial_t \mathbf{u} \cdot \boldsymbol{\omega} \, dx + \int_\Omega \mathbf{u} \cdot \nabla \times \partial_t \mathbf{u} \, dx = 2 \int_\Omega \partial_t \mathbf{u} \cdot \boldsymbol{\omega} \, dx \\ &= 2 \int_\Omega \left(\mathbf{u} \times \boldsymbol{\omega} + R_e^{-1} \nabla \times \nabla \times \mathbf{u} - \nabla \left(\frac{1}{2} |\mathbf{u}|^2 + \tilde{p} \right) + \mathbf{f} \right) \cdot \boldsymbol{\omega} \, dx \\ &= 2 \int_\Omega (R_e^{-1} \nabla \times \nabla \times \mathbf{u} + \mathbf{f}) \cdot \boldsymbol{\omega} \, dx \end{aligned}$$

This completes the proof. □

This theorem tells that for the ideal case when $R_e = \infty$ and $\mathbf{f} = \mathbf{0}$, we obtain the helicity conservation. On the other hand, the natural pollution term for the helicity conservation is the effect of diffusion. Therefore, throughout the discussion that follows, we shall assume $\mathbf{f} = \mathbf{0}$.

2.1 Finite element preserving the fluids helicity

In this section, we shall consider Helicity-conservative finite element methods defined on contractible domains. One can extend the definition of helicity to nontrivial topology and different space dimensions [3, Chapter 3]. We use the standard notation for the inner product and the norm of the L^2 space

$$(u, v) := \int_{\Omega} u \cdot v dx, \quad \|u\|_0 := \left(\int_{\Omega} |u|^2 dx \right)^{1/2}.$$

Define the following $H(D, \Omega)$ space with a given linear operator D :

$$H(D, \Omega) := \{v \in L^2(\Omega), Dv \in L^2(\Omega)\},$$

and

$$H_0(D, \Omega) := \{v \in H(D, \Omega), t_D v = 0 \text{ on } \partial\Omega\},$$

where t_D is the trace operator:

$$t_D v := \begin{cases} v, & D = \text{grad}, \\ v \times n, & D = \text{curl}, \\ v \cdot n, & D = \text{div}. \end{cases}$$

We also define:

$$L_0^2(\Omega) := \left\{ v \in L^2(\Omega) : \int_{\Omega} v = 0 \right\}.$$

By definition, $H_0(\text{grad}, \Omega)$ coincides with $H_0^1(\Omega)$.

The de Rham complex in three space dimensions with vanishing boundary conditions reads:

$$0 \longrightarrow H_0(\text{grad}, \Omega) \xrightarrow{\text{grad}} H_0(\text{curl}, \Omega) \xrightarrow{\text{curl}} H_0(\text{div}, \Omega) \xrightarrow{\text{div}} L_0^2(\Omega) \longrightarrow 0. \quad (2.8)$$

The sequence (2.8) is exact on contractible domains, meaning that $\mathcal{N}(\text{curl}) = \mathcal{R}(\text{grad})$ and $\mathcal{N}(\text{div}) = \mathcal{R}(\text{curl})$, where \mathcal{N} and \mathcal{R} denote the kernel and range of an operator, respectively.

A main idea of the discrete differential forms [1, 2] or the finite element exterior calculus [6, 12] is to construct finite elements for the spaces in (2.8) such that they fit into a discrete sequence

$$0 \longrightarrow H_0^h(\text{grad}, \Omega) \xrightarrow{\text{grad}} H_0^h(\text{curl}, \Omega) \xrightarrow{\text{curl}} H_0^h(\text{div}, \Omega) \xrightarrow{\text{div}} L_0^{2,h}(\Omega) \longrightarrow 0. \quad (2.9)$$

The discrete de Rham sequences can be of arbitrary order [5, 2]. Figure 1 shows the finite elements of the lowest order (Whitney forms).

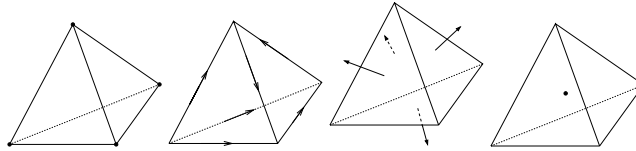


Figure 1: DOFs of the finite element de Rham sequence of lowest order

Throughout this section, we shall use $\mathbb{Q}_h^{\text{curl}}$, the L^2 projection onto $H_0^h(\text{curl}, \Omega)$:

$$\mathbb{Q}_h^{\text{curl}} : [L^2(\Omega)]^3 \mapsto H_0^h(\text{curl}, \Omega) \quad (2.10)$$

and the operator $\nabla_h \times : H_0^h(\text{div}, \Omega) \mapsto H_0^h(\text{curl}, \Omega)$ defined by the following relation:

$$(\nabla_h \times \mathbf{U}, \mathbf{V}) = (\mathbf{U}, \nabla \times \mathbf{V}) \quad \forall (\mathbf{U}, \mathbf{V}) \in H_0^h(\text{div}, \Omega) \times H_0^h(\text{curl}, \Omega). \quad (2.11)$$

We are now in a position to present the helicity-preserving full discretization for the Navier-Stokes system. Generally, for helicity preserving scheme, mid-point method in time discretization is used [18, 28]. We shall define

$$\mathbf{X}_h = H_0^h(\text{curl}, \Omega) \times H_0^h(\text{curl}, \Omega) \times H_0^h(\text{grad}). \quad (2.12)$$

The scheme can be written as follows: find $(\mathbf{u}, \boldsymbol{\omega}, p) \in \mathbf{X}_h$, such that for all $(\mathbf{v}, \boldsymbol{\mu}, q) \in \mathbf{X}_h$:

$$(D_t \mathbf{u}, \mathbf{v}) - (\mathbf{u} \times \boldsymbol{\omega}, \mathbf{v}) + R_e^{-1}(\nabla \times \mathbf{u}, \nabla \times \mathbf{v}) + (\nabla p, \mathbf{v}) = (\mathbf{0}, \mathbf{v}), \quad (2.13a)$$

$$(\boldsymbol{\omega}, \boldsymbol{\mu}) - (\nabla \times \mathbf{u}, \boldsymbol{\mu}) = 0, \quad (2.13b)$$

$$(\mathbf{u}, \nabla q) = 0, \quad (2.13c)$$

where

$$D_t \mathbf{u} := \frac{\mathbf{u}^{n+1} - \mathbf{u}^n}{\Delta t}, \quad (2.14)$$

and all the unknowns without time derivative, i.e., $\mathbf{u}, \boldsymbol{\omega}, p$ are defined at the midpoint in time interval $[t_n, t_{n+1}]$, e.g.,

$$\mathbf{u} = \frac{\mathbf{u}^{n+1} + \mathbf{u}^n}{2}. \quad (2.15)$$

We note that this weak form can be equivalently formulated as to find $\mathbf{u}, \boldsymbol{\omega}, p \in \mathbf{X}_h$ such that

$$D_t \mathbf{u} - \mathbb{Q}_h^{\text{curl}}(\mathbf{u} \times \mathbb{Q}_h^{\text{curl}}[\nabla \times \mathbf{u}]) + \nabla p + R_e^{-1} \nabla_h \times \nabla \times \mathbf{u} = \mathbf{0}. \quad (2.16)$$

We shall now list some of properties and the helicity conservation holds in a very limited case. We first introduce a simple but important lemma, whose proof can be found at [14]:

Lemma 1. For any given $\boldsymbol{\xi} \in \mathbb{R}^3$, we have

$$(D_t \boldsymbol{\xi}, \boldsymbol{\xi}) = \frac{1}{2\Delta t} (\|\boldsymbol{\xi}^{n+1}\|^2 - \|\boldsymbol{\xi}^n\|^2). \quad (2.17)$$

Furthermore, for any pair of vectors $(\boldsymbol{\xi}, \boldsymbol{\nu}) \in \mathbb{R}^3 \times \mathbb{R}^3$, we have the following identity:

$$D_t \int \boldsymbol{\xi} \cdot \boldsymbol{\nu} = \int D_t \boldsymbol{\xi} \cdot \boldsymbol{\nu} + \int \boldsymbol{\xi} \cdot D_t \boldsymbol{\nu}, \quad (2.18)$$

where

$$D_t \int \boldsymbol{\xi} \cdot \boldsymbol{\nu} := \frac{1}{\Delta t} \left(\int \boldsymbol{\xi}^{n+1} \cdot \boldsymbol{\nu}^{n+1} - \int \boldsymbol{\xi}^n \cdot \boldsymbol{\nu}^n \right). \quad (2.19)$$

We now show the energy law for (2.13):

Theorem 3. The discrete energy law holds:

$$(D_t \mathbf{u}, \mathbf{u}) + R_e^{-1} \|\nabla \times \mathbf{u}\|^2 = 0. \quad (2.20)$$

We shall now discuss the fluid helicity. The following theorems can be similarly stated and proved for any contractible subdomain $\tilde{\Omega} \subset \Omega$ if the variables satisfy the boundary conditions (2.2), or even weaker conditions, on the boundary of $\tilde{\Omega}$. Therefore we obtain identities for both local and global helicity. For simplicity of presentation, we focus on the helicity on Ω , i.e., the global helicity, and stick to the boundary conditions (2.2).

Theorem 4. Any solution for (2.13) satisfies the following identity for the fluid helicity:

$$D_t \int_{\Omega} \mathbf{u} \cdot \boldsymbol{\omega} = -2R_e^{-1} \int_{\Omega} \nabla \times \mathbf{u} \cdot \nabla \times \boldsymbol{\omega}. \quad (2.21)$$

Proof. We note the following discrete weak form in the following formulation:

$$D_t \mathbf{u} - \mathbb{Q}_h^{\text{curl}}(\mathbf{u} \times \mathbb{Q}_h^{\text{curl}}[\nabla \times \mathbf{u}]) + \nabla p + R_e^{-1} \nabla_h \times \nabla \times \mathbf{u} = \mathbf{0}. \quad (2.22)$$

We note that we can define the fluid helicity using either the total integral of $\mathbf{u} \cdot \nabla \times \mathbf{u}$ or $\mathbf{u} \cdot \boldsymbol{\omega}$, for both of which, we note that the following holds:

$$\begin{aligned} D_t \int_{\Omega} \mathbf{u} \cdot \boldsymbol{\omega} &= \int_{\Omega} D_t \mathbf{u} \cdot \boldsymbol{\omega} + \int_{\Omega} \mathbf{u} \cdot D_t \boldsymbol{\omega} = 2 \int_{\Omega} D_t \mathbf{u} \cdot \boldsymbol{\omega} \\ &= 2 \left[\int_{\Omega} [\mathbf{u} \times \mathbb{Q}_h^{\text{curl}}(\nabla \times \mathbf{u})] \cdot \boldsymbol{\omega} + \int_{\Omega} \nabla p \cdot \boldsymbol{\omega} - R_e^{-1} \int_{\Omega} \nabla \times \mathbf{u} \cdot \nabla \times \boldsymbol{\omega} \right] \\ &= -2R_e^{-1} \int_{\Omega} \nabla \times \mathbf{u} \cdot \nabla \times \boldsymbol{\omega}. \end{aligned}$$

This implies the desired result. \square

We remark that in Girault, the following finite element scheme has been introduced [11]: find $(\mathbf{u}, p) \in H_0^h(\text{curl}, \Omega) \times H_0^h(\text{grad})$, such that for all $(\mathbf{v}, \boldsymbol{\mu}, q) \in H_0^h(\text{curl}, \Omega) \times H_0^h(\text{grad})$:

$$(D_t \mathbf{u}, \mathbf{v}) - (\mathbf{u} \times \nabla \times \mathbf{u}, \mathbf{v}) + R_e^{-1} (\nabla \times \mathbf{u}, \nabla \times \mathbf{v}) + (\nabla p, \mathbf{v}) = (\mathbf{f}, \mathbf{v}), \quad (2.23a)$$

$$(\mathbf{u}, \nabla q) = 0, \quad (2.23b)$$

subject to the same boundary condition with the scheme. However, we can see that this scheme does not preserve helicity (see Figure 9 below).

3 Helicity-conservative PINN models

We shall now look at the PINN model, which uses the strong form of PDE as a loss function. We continue to consider the following 3D Navier-Stokes equation with initial condition as given in (2.1). On the other hand, for the helicity conservation, we shall assume that the external force is zero. Therefore, we shall assume $\mathbf{f} = \mathbf{0}$.

We note that we are training $p = \frac{1}{2} |\mathbf{u}|^2 + \tilde{p}$, \tilde{p} is the output p_{NN} of PINN, and p is the modified pressure. Our model minimizes the following functionals for finding \mathbf{u}_{NN} and p_{NN} . Initially, the term of initial condition of \mathbf{u} and p is:

$$\mathcal{L}_{\text{init}(\mathbf{u}, p)} = \frac{1}{N_0} \sum_{i=1}^{N_0} \left(\|\mathbf{u}(t^i, \mathbf{x}^i) - \mathbf{u}^i\|_0^2 + |p(t^i, \mathbf{x}^i) - p^i|^2 \right), \quad (3.1)$$

where N_0 is the number of sampling points for initial condition, and $\mathbf{u}_{NN} = (\mathbf{u}^i = \{u_1^i, u_2^i, u_3^i\})_{i=1}^{i=N_0}$ and $p_{NN} = (p^i)_{i=1}^{i=N_0}$ denote the initial training data on

$$\mathbf{u}(t^i, \mathbf{x}^i) = \{u_1(t^i, x^i, y^i, z^i), u_2(t^i, x^i, y^i, z^i), u_3(t^i, x^i, y^i, z^i)\} \quad (3.2)$$

and $p(t^i, x^i, y^i, z^i)$ for $i = 1, \dots, N_0$. Now, the loss function for boundary conditions can be defined according to (2.2):

$$\mathcal{L}_{\text{bdry}(u,p)} = \frac{1}{N_b} \sum_{i=1}^{N_b} \left(\|\mathbf{u}^i \times \mathbf{n}\|_0^2 + \left(\frac{1}{2} \|\mathbf{u}^i\|_0 + \tilde{p}^i \right)^2 \right), \quad (3.3)$$

where N_b is the number of sampling points for boundary condition. Next we consider the loss function for the momentum equation as well as the loss function for the divergence free condition for \mathbf{u} , respectively as follows:

$$\mathcal{L}_{\text{momentum}} = \frac{1}{N_f} \sum_{i=1}^{N_m} \left(\partial_t \mathbf{u}^i - \mathbf{u}^i \times \nabla \times \mathbf{u}^i + R_e^{-1} \nabla \times \nabla \times \mathbf{u}^i + \nabla p^i \right)^2, \quad (3.4a)$$

$$\mathcal{L}_{\text{divergence}} = \frac{1}{N_f} \sum_{i=1}^{N_f} |\text{div} \mathbf{u}^i|^2, \quad (3.4b)$$

where N_f is the number of sampling points for the equation. The functional that the PINN model to optimize is given as follows:

$$\min_{\mathbf{u}_{NN}, p_{NN}} \mathcal{L}_{\text{init}(u,p)} + \mathcal{L}_{\text{bdry}} + \mathcal{L}_{\text{momentum}} + \mathcal{L}_{\text{divergence}} \quad (3.5)$$

The original PINN approach trains the NN model to predict the entire space-time at once. In complex cases, this can be more difficult to learn. Seq2seq strategy was proposed in [16], where the PINN learns to predict the solution at each time step, instead of all times. Note that the only data available of the first sequence is from the PDE itself, i.e., just the initial condition. We take the prediction at $t = \Delta t$ by using the model of the first sequence and use this as the initial condition to make a prediction in the next sequence, and so on. which can be shown in Figure 2.

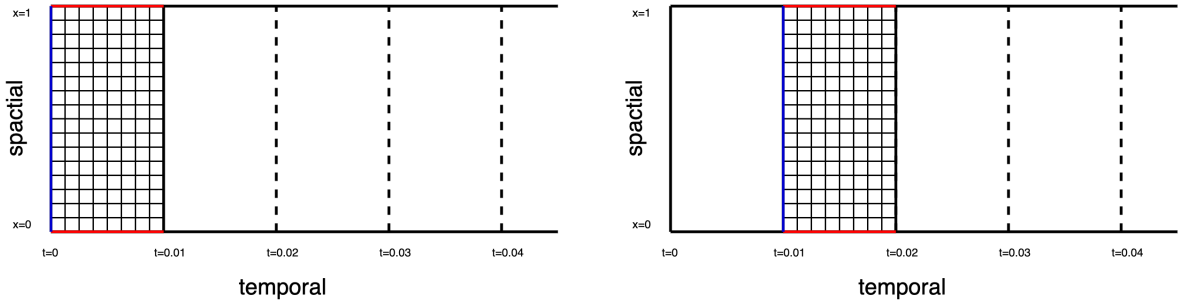


Figure 2: Seq2seq PINN. The blue line is initial condition for each sequence. The red line is boundary condition for each sequence. The domain will be uniformly sectioned. When training of the first sequence finished, the solution at $t = 0.01$ will be calculated and used as the initial condition for the next sequence.

After training our model, we'll calculate whether the helicity conserves. The helicity is defined as follows. Here we use Gaussian quadrature to replace the integral.

$$\mathcal{H}_f = \int_{\Omega} \mathbf{u} \cdot \nabla \times \mathbf{u} \, dx \quad (3.6)$$

Computationally, we want realize it using the neural network function as follows:

$$\mathcal{H}_f = \int_{\Omega} \mathbf{u}_{NN} \cdot \nabla \times \mathbf{u}_{NN} \, dx, \quad (3.7)$$

where $\omega = \nabla \times \mathbf{u}_{NN}$. In conclusion, our helicity-conservative PINN model shows as Algorithm 1

Algorithm 1 Helicity-conservative PINN model

- 1: **Input:** Initial sample points for \mathbf{u} , p and sample points in Ω for numerical integration and training algorithm, and the number of layers L , the final time level T and the time domain of one sequence dT .
 - 2: **Output:** \mathbf{u} , w , p in the sample points in Ω .
 - 3: Initialize PINN model parameters, weights and bias denoted by $(\mathbf{W}^{1,(0)}, \dots, \mathbf{W}^{L,(0)})$ and $(\mathbf{b}^{1,(0)}, \dots, \mathbf{b}^{L,(0)})$
 - 4: Generate initial points and corresponding \mathbf{u} , w , p
 - 5: **for** seq=1, \dots , T/dT **do**
 - 6: Generate sample points in Ω
 - 7: **repeat**
 - 8: Compute \mathbf{u} and p using neural network, and then $\omega = \nabla \times \mathbf{u}$
 - 9: Compute loss of initial condition
 - 10: Compute loss of boundary condition
 - 11: Compute loss of equation
 - 12: $Loss = \mathcal{L}_{init_{NN}} + \mathcal{L}_{bdry(\mathbf{u}, p)} + \mathcal{L}_{momentum} + \mathcal{L}_{divergence}$
 - 13: Optimize $Loss$ based on **Adam** \triangleright Learning rate of **Adam** changes depending on $Loss$
 - 14: **until** $Loss < \text{particular number}$
 - 15: Compute helicity \mathcal{H}_f $\triangleright \mathcal{H}_f = \int_{\Omega} \mathbf{u} \cdot \omega \, dx$
 - 16: Compute \mathbf{u} , w , p at the end of this sequence, used as initial condition for next sequence
-

Theorem 5. *The Algorithm 1 admits the neural network solution $(\mathbf{u}_{NN}, p_{NN})$ that satisfies the following identity for the fluid helicity:*

$$D_t Q_{\Omega}(\mathbf{u}_{NN} \cdot \nabla \times \mathbf{u}_{NN}) = -2R_e^{-1} Q_{\Omega}(\nabla \times \mathbf{u}_{NN} \cdot \nabla \times \nabla \times \mathbf{u}_{NN}) + 2Q_{\Omega}(\nabla p_{NN} \cdot \omega).$$

Proof. We note the following discrete weak form in the following formulation:

$$D_t \mathbf{u} - (\mathbf{u} \times [\nabla \times \mathbf{u}]) + \nabla p + R_e^{-1} \nabla \times \nabla \times \mathbf{u} = \mathbf{0}, \quad \forall (t^i, \mathbf{x}^i) \in (0, T] \times \Omega. \quad (3.8)$$

This leads to

$$\begin{aligned} D_t \mathbf{u} \cdot \omega &= D_t \mathbf{u} \cdot \omega + \mathbf{u} \cdot D_t \omega = 2D_t \mathbf{u} \cdot \omega \\ &= 2[(\mathbf{u} \times \nabla \times \mathbf{u}) \cdot \omega + \nabla p \cdot \omega - R_e^{-1} \nabla \times \mathbf{u} \cdot \nabla \times \omega] \\ &= 2\nabla p \cdot \omega - 2R_e^{-1} \nabla \times \mathbf{u} \cdot \nabla \times \omega. \end{aligned}$$

By taking numerical quadrature rule to define the fluid helicity, we obtain the desired result and this completes the proof. \square

Corollary 1. *If the integral Q_{Ω} is done accurately and $R_e = \infty$, then the helicity from Algorithm 1 is conserved exactly.*

$$D_t \int_{\Omega} (\mathbf{u}_{NN} \cdot \nabla \times \mathbf{u}_{NN}) \, dx = 0.$$

Proof. We assume that the integral is computed exactly. Then, we have that

$$Q_\Omega(\nabla p \cdot \boldsymbol{\omega}) = \int_\Omega \nabla p \cdot \boldsymbol{\omega} \, dx = - \int_\Omega p \operatorname{div} \boldsymbol{\omega} \, dx + \int_{\partial\Omega} p \cdot \mathbf{n} \boldsymbol{\omega} \, ds = 0. \quad (3.9)$$

The last equality is due to the fact that $\boldsymbol{\omega}$ is divergence-free. This completes the proof. \square

Helicity-conservative PINN model should preserve the initial helicity value in the time evolution. For demonstrating the helicity conservative property of Helicity-conservative PINN model, We describe the algorithm based on Girault [11] as ω_{NN} Network. In ω_{NN} Network, the following form of the equation is considered:

$$\begin{aligned} \partial_t \mathbf{u}_{NN} - \mathbf{u}_{NN} \times \boldsymbol{\omega}_{NN} + R_e^{-1} \nabla \times \nabla \times \mathbf{u}_{NN} + \nabla p_{NN} &= \mathbf{0}, \\ \boldsymbol{\omega}_{NN} - \nabla \times \mathbf{u}_{NN} &= \mathbf{0}, \end{aligned} \quad (3.10)$$

This means the initial, boundary and divergence-free condition are all the same as Helicity-conservative PINN model, except that in ω_{NN} Network, $\boldsymbol{\omega}$ is directly generated by neural network, rather than calculated by \mathbf{u} . In summary, the difference between Helicity-conservative PINN model and ω_{NN} network is as follows. First, the loss of initial $\boldsymbol{\omega}$ should be computed directly, rather than $\boldsymbol{\omega} = \nabla \times \mathbf{u}$. Second, the loss of $\boldsymbol{\omega}$ should be added, which is:

$$\mathcal{L}_\omega = \frac{1}{N_f} \sum_{i=1}^{N_f} \|\boldsymbol{\omega}^i - \nabla \times \mathbf{u}^i\|_0^2. \quad (3.11)$$

Third, the loss function for the momentum equation should be:

$$\mathcal{L}_{\text{momentum}} = \frac{1}{N_f} \sum_{i=1}^{N_m} (\partial_t \mathbf{u}^i - \mathbf{u}^i \times \boldsymbol{\omega}^i + R_e^{-1} \nabla \times \nabla \times \mathbf{u}^i + \nabla p^i)^2. \quad (3.12)$$

In conclusion, the algorithm of ω_{NN} Network is presented as Algorithm 2.

Theorem 6. *The Algorithm 2 admits the neural network solution $(\mathbf{u}_{NN}, \boldsymbol{\omega}_{NN}, p_{NN})$ that satisfies the following identity for the fluid helicity:*

$$D_t Q_\Omega(\mathbf{u}_{NN} \cdot \boldsymbol{\omega}_{NN}) = -2R_e^{-1} Q_\Omega(\nabla \times \mathbf{u}_{NN} \cdot \nabla \times \nabla \times \mathbf{u}_{NN}) + 2Q_\Omega(\nabla p_{NN} \cdot \boldsymbol{\omega}_{NN}). \quad (3.13)$$

Proof. Similarly to the Algorithm 1, we can have the following discrete identity since neural network functions and their derivatives can represent zero:

$$D_t \mathbf{u} - (\mathbf{u} \times [\nabla \times \mathbf{u}]) + \nabla p + R_e^{-1} \nabla \times \nabla \times \mathbf{u} = \mathbf{0}. \quad (3.14)$$

We note that we can define the fluid helicity using either the total integral of $\mathbf{u} \cdot \boldsymbol{\omega}$ as follows:

$$\begin{aligned} D_t Q_\Omega(\mathbf{u} \cdot \boldsymbol{\omega}) &= Q_\Omega(D_t \mathbf{u} \cdot \boldsymbol{\omega}) + Q_\Omega(\mathbf{u} \cdot D_t \boldsymbol{\omega}) = 2Q_\Omega(D_t \mathbf{u} \cdot \boldsymbol{\omega}) \\ &= 2 [Q_\Omega([\mathbf{u} \times \boldsymbol{\omega}] \cdot \boldsymbol{\omega}) + Q_\Omega(\nabla p \cdot \boldsymbol{\omega}) - R_e^{-1} Q_\Omega(\nabla \times \mathbf{u} \cdot \nabla \times \boldsymbol{\omega})] \\ &= -2R_e^{-1} Q_\Omega(\nabla \times \mathbf{u} \cdot \nabla \times \boldsymbol{\omega}) + 2Q_\Omega(\nabla p \cdot \boldsymbol{\omega}). \end{aligned}$$

This implies the desired result. \square

Algorithm 2 ω_{NN} Network

- 1: **Input:** Initial sample points for u, ω, p and sample points in Ω for numerical integration and training algorithm, and the number of layers L , the final time level T and the time domain of one sequence dT .
 - 2: **Output:** u, w, p in the sample points in Ω .
 - 3: Initialize PINN model parameters, weights and bias denoted by $(W^{1,(0)}, \dots, W^{L,(0)})$ and $(b^{1,(0)}, \dots, b^{L,(0)})$
 - 4: Generate initial points and corresponding u, w, p
 - 5: **for** seq=1, \dots , T/dT **do**
 - 6: Generate scattered points in domain
 - 7: **repeat**
 - 8: Compute u, ω and p using neural network.
 - 9: Compute loss of initial condition
 - 10: Compute loss of ω
 - 11: Compute loss of boundary condition
 - 12: Compute loss of equation
 - 13: $Loss = \mathcal{L}_{init_{NN}} + \mathcal{L}_{\omega} + \mathcal{L}_{bdry(u,p)} + \mathcal{L}_{momentum} + \mathcal{L}_{divergence}$
 - 14: Optimize $Loss$ based on **Adam** \triangleright Learning rate of **Adam** changes depending on $Loss$
 - 15: **until** $Loss < \text{particular number}$
 - 16: Compute helicity \mathcal{H}_f $\triangleright \mathcal{H}_f = \int_{\Omega} u \cdot \omega \, dx$
 - 17: Compute u, w, p at the end of this sequence, used as initial condition for next sequence
-

The difference in the helicity expression from Algorithm 1 and Algorithm 2 can be found at the term

$$Q_{\Omega}(\nabla p_{NN} \cdot \nabla \times u_{NN}) \quad \text{and} \quad Q_{\Omega}(\nabla p_{NN} \cdot \nabla \times w_{NN}). \quad (3.15)$$

The crucial point we make is that even if we obtain the best possible optimizer in Algorithm 2, it is in general impossible to make the loss function for the vorticity zero since ω_{NN} can not represent $\nabla \times u_{NN}$. In fact the best possible ω_{NN} is given as follows:

$$\omega_{NN} = Q_{NN}(\nabla \times u_{NN}), \quad (3.16)$$

where Q_{NN} is the L^2 projection onto the space of neural network functions chosen in the model. This in general can not guarantee the divergence free property of ω_{NN} and thus the helicity conservation of Algorithm 2 may not hold in general. Therefore, we arrive at the following similar but different corollary. By taking numerical quadrature rule to define the fluid helicity, we obtain the desired result and this completes the proof.

Corollary 2. *If the integral Q_{Ω} is done accurately and $R_e = \infty$, then the helicity is not in general conserved exactly for Algorithm 2. More precisely, we have that:*

$$D_t \int_{\Omega} (u_{NN} \cdot w_{NN}) \, dx = 2 \int_{\Omega} \nabla p_{NN} \cdot \omega_{NN} \, dx.$$

4 Numerical Experiments

We now report a couple of numerical tests. One result is the error analysis with analytic solutions. The other is to show that the proposed scheme can conserve the helicity. The numerical experiments are performed on a workstation with 1 10 Core Intel(R) Xeon(R) Silver 4210R CPU, 1 RTX A5000 GPU, 128GB RAM, and a Ubuntu 20.04 operating system that implements Pytorch. Note that we choose Adam as the optimizer and the learning rate is different depending on the loss term (3.5). In this case, the training process will guarantee both convergence and speed. We use \tanh as the activation function. In series of experiments, we choose $h = 1/16$ and $\Delta t = 1e - 3$ when calculating Gaussian quadrature in order to guarantee the fairness of evaluation criterion.

4.1 Error Analysis with analytic solution

In this section, we carry out a 3D error test with the following form of solutions on the domain $\Omega = [0, 1]^3$. First we generate analytic solutions of the equation. starting at

$$\tilde{p} = h(x)h(y)h(z), \quad (4.1)$$

where $h(\mu) = (\mu^2 - \mu)^2$. Further, we let

$$g_1(t) = 4 - 2t, \quad g_2(t) = 1 + t \quad \text{and} \quad g_3(t) = 1 - t. \quad (4.2)$$

We now introduce analytic velocity that satisfy the boundary conditions. Namely,

$$\mathbf{u} = \begin{pmatrix} -g_1 h'(x)h(y)h(z) \\ -g_2 h(x)h'(y)h(z) \\ -g_3 h(x)h(y)h'(z) \end{pmatrix}.$$

With this setting, $\mathbf{u} \times \mathbf{n} = 0$, and the modified pressure $p = |\mathbf{u}|^2/2 + \tilde{p}$ satisfies the boundary condition.

We report the numerical error analysis obtained by solving Navier-Stokes equation obtained by setting $R_e = 10^4$ for the model problem. The interval of the mesh $h = 1/16$ and the whole time domain $T = 1s$. The time domain of each sequence is $0.01s$ and the time interval of each sequence $\Delta t = 1e - 3s$. The L_2 error is shown in Table 1.

$\ \mathbf{u} - \mathbf{u}_h\ _{L_2}$	$\ \boldsymbol{\omega} - \boldsymbol{\omega}_h\ _{L_2}$	$\ p - p_h\ _{L_2}$
5.029E-04	7.584E-04	2.369E-04

Table 1: Numerical Error Analysis for solving Navier-Stokes equation. The time level at which the error is computed is $T = 1$ and $dt = 1e - 03$. $R_e = 10^4$.

In order to show the effect of different space intervals and time intervals, two groups of comparison tests have been done. First, we choose different space interval h to observe the performance of our model. Table 2 shows the result of different h .

h	$\ \mathbf{u} - \mathbf{u}_h\ _{L_2}$	$\ \boldsymbol{\omega} - \boldsymbol{\omega}_h\ _{L_2}$	$\ p - p_h\ _{L_2}$
2^{-2}	8.315E-03	4.264E-02	1.564E-04
2^{-3}	1.621E-03	2.331E-03	3.996E-04
2^{-4}	5.029E-04	7.584E-04	2.369E-04

Table 2: Error analysis of different h while $\Delta t = 1e-03$. The time level at which the error is computed is $T = 1$. $R_e = 10^4$.

Then we choose different time interval Δt to observe the performance of our model. Table 3 shows the result of different Δt . We can conclude that the space interval has more influence to the error than the time interval.

Δt	$\ \mathbf{u} - \mathbf{u}_h\ _{L_2}$	$\ \boldsymbol{\omega} - \boldsymbol{\omega}_h\ _{L_2}$	$\ p - p_h\ _{L_2}$
2E-3	5.618E-04	7.604E-04	1.334e-04
1E-3	5.029E-04	7.584E-04	2.369E-04
5E-4	5.556E-04	7.597E-04	5.900E-06

Table 3: Error analysis of different Δt while $h = 1/16$. The time level at which the error is computed is $T = 1$. $R_e = 10^4$.

4.2 Tests for Helicity conservation

In this section, we test our algorithm for conservation of divergence(Div), energy(E_f) and fluid helicity(\mathcal{H}_f). Our initial condition is given for \mathbf{u} , $\boldsymbol{\omega}$ and p as follows:

$$\begin{aligned}
u_1 &= -\sin(\pi(x-0.5))\cos(\pi(y-0.5))z(z-1), \\
u_2 &= \cos(\pi(x-0.5))\sin(\pi(y-0.5))z(z-1), \\
u_3 &= 0, p = 0.
\end{aligned} \tag{4.3}$$

As depicted in Figure 3 below, we note that the desired boundary conditions are satisfied:

$$\mathbf{u} \times \mathbf{n} = 0, \text{ on } \partial\Omega. \tag{4.4}$$

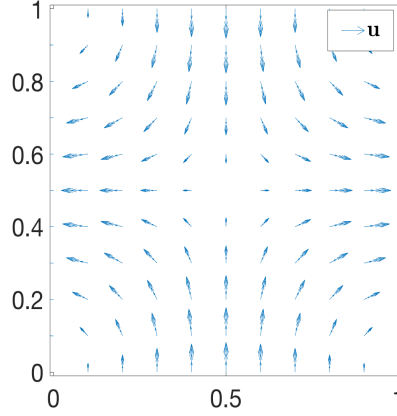


Figure 3: Top view, or projection (onto xy plane) of initial u

For the pressure $p = \tilde{p} + \frac{1}{2}|u|^2$, we impose the zero boundary condition. Besides, $f = 0$ in this test. Under this setting, we first show that the divergence conserves well. The divergence is defined as the maximum divergence at certain times, which is shown as Figure 4. The result presents that our model satisfies the divergence-free condition well.

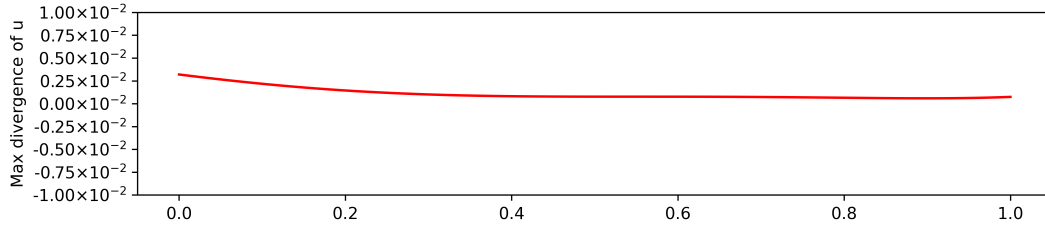


Figure 4: Maximum divergence of u for $T = 1s$

More importantly, we can show that the followings hold true at the limit, when R_e approaches ∞ , the energy conserves. which means:

$$\|u\|_{L_2} = \sqrt{\int_{\Omega} |u|^2 dx} = 0, \quad \forall t \in [0, \infty).$$

Energy conservation experiment is shown as Figure 5. The figure indicates that $\|u\|_{L_2}$ approaches to 0, which means the energy conserves well.

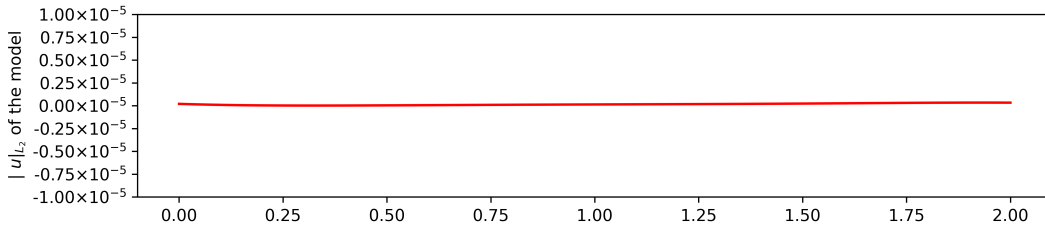


Figure 5: Energy conserves when $T = 1s$

Additionally, the helicity also conserves:

$$\mathcal{H}_f(t) = \int_{\Omega} \mathbf{u} \cdot \boldsymbol{\omega} \, dx = 0, \quad \forall t \in [0, \infty).$$

We call Algorithm 1 as up_{NN} Network and Algorithm 2 as ω_{NN} Network. In 3.9, $\text{div}\boldsymbol{\omega}$ is the most significant term for making the formula zero. Divergence of $\boldsymbol{\omega}$ shows as Figure 6. This verifies that the divergence of $\boldsymbol{\omega}$ is the main reason fails to conserve the helicity for ω_{NN} Network.

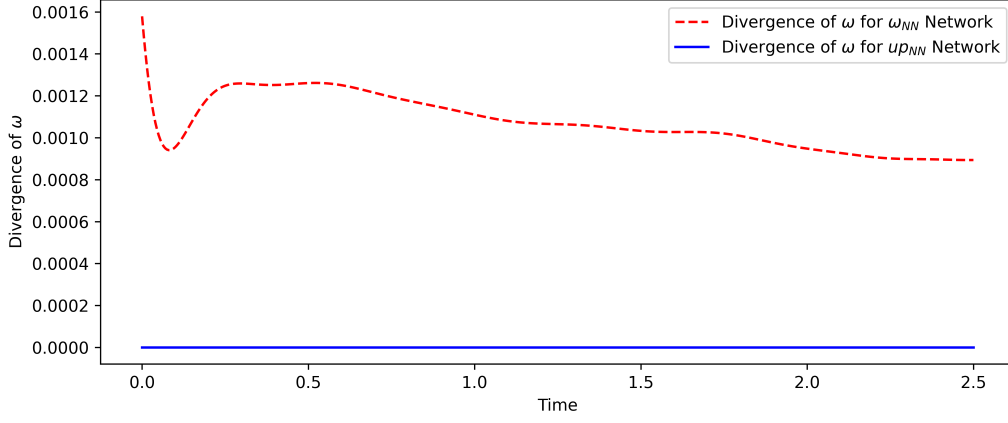


Figure 6: Maximum divergence of $\boldsymbol{\omega}$ for $T = 2.5s$

Further more, 3.13 presents that $\int \nabla p \cdot \boldsymbol{\omega}$ is the key that ω_{NN} Network fails to preserve the helicity. It is shown as Figure 7, which indicates that the $\int \nabla p \cdot \boldsymbol{\omega}$ of up_{NN} Network conserves well but ω_{NN} Network is not.

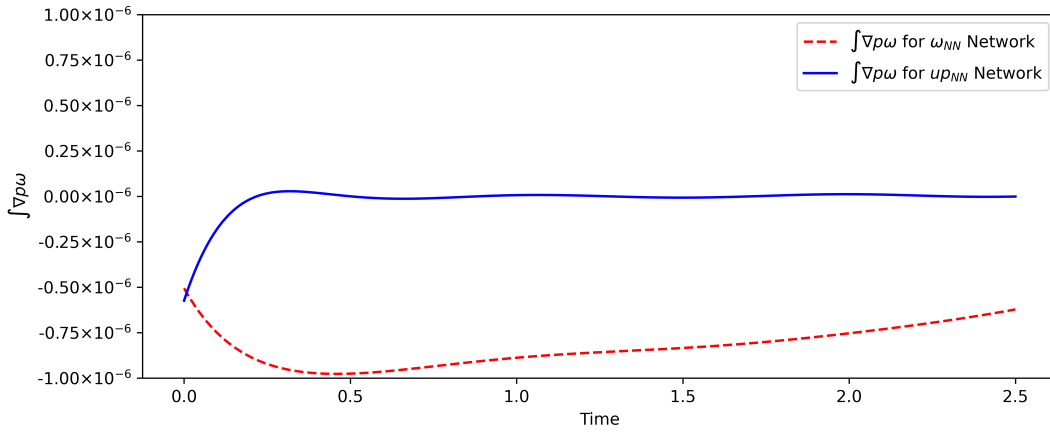


Figure 7: $\int \nabla p \cdot \boldsymbol{\omega}$ for $T = 2.8s$

Experiments show that our scheme preserves the helicity orders of magnitude better with a simple modification in the definition of the vorticity. Figure 8 show that the helicity of our model

conserves better. Besides, when the interval of mesh becomes larger, the helicity fails to conserve as well as the refining one.

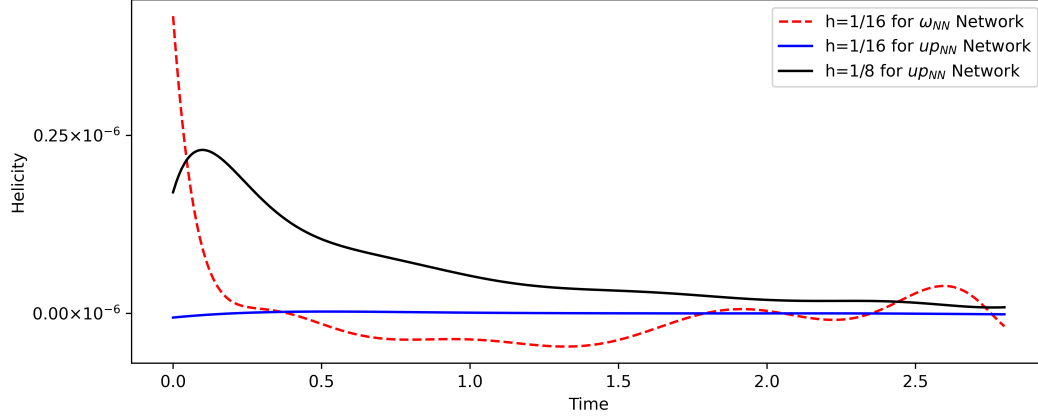


Figure 8: Helicity conservation when $T = 2.5s$

Figure 9 shows that the finite element scheme mentioned in [11] does not preserve helicity. But our finite element method introduced in section 2.1 conserves the helicity.

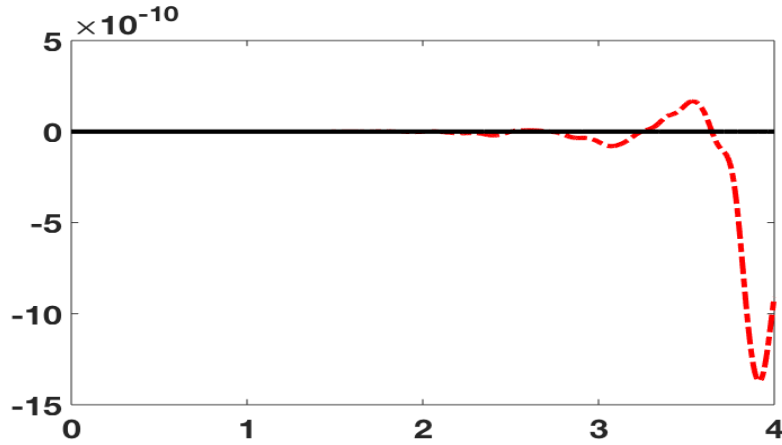


Figure 9: \mathcal{H}_f for Girault method (red, dot line) and our finite element method (black, solid line) at $Re = 10^6$ with $h = 1/16$ and $\Delta t = 1/1000$.

5 Conclusion

Neural network is popular and it has a lot of potential. In this paper, we provide a first attempt to use neural network function to preserve helicity of Navier-Stokes equation. Our observation is that PINN model is based on the strong form of PDE, it is easier to demonstrate the conservation

property unlike the weak form of PDE. In the forthcoming paper, we shall solve MHD equation that preserves the magnetic and cross helicities.

Acknowledgement

Authors thank Jinchao Xu and Kaibo Hu for helpful discussion.

References

- [1] Douglas N Arnold. *Finite element exterior calculus*, volume 93. SIAM, 2018.
- [2] Douglas N Arnold, Richard S Falk, and Ragnar Winther. Finite element exterior calculus, homological techniques, and applications. *Acta numerica*, 15:1, May 2006.
- [3] Vladimir I Arnold and Boris A Khesin. *Topological methods in hydrodynamics*, volume 125. Springer Science & Business Media, 1999.
- [4] Mitchell A Berger and George B Field. The topological properties of magnetic helicity. *Journal of Fluid Mechanics*, 147:133–148, 1984.
- [5] D. Boffi, F. Brezzi, and M. Fortin. *Mixed Finite Element Methods and Applications*. Springer, 2013.
- [6] A. Bossavit. *Computational Electromagnetism*. Academic Press (Boston), 1998.
- [7] Jason Cantarella, Dennis DeTurck, Herman Gluck, and Mikhail Teytel. Influence of geometry and topology on helicity. *Geophysical Monograph-American Geophysical Union*, 111:17–24, 1999.
- [8] Uriel Frisch, A Pouquet, J L  orat, and A Mazure. Possibility of an inverse cascade of magnetic helicity in magnetohydrodynamic turbulence. *Journal of Fluid Mechanics*, 68(4):769–778, 1975.
- [9] Evan S Gawlik and Fran  ois Gay-Balmaz. A variational finite element discretization of compressible flow. *arXiv preprint arXiv:1910.05648*, 2019.
- [10] Evan S Gawlik and Fran  ois Gay-Balmaz. A conservative finite element method for the incompressible Euler equations with variable density. *Journal of Computational Physics*, page 109439, 2020.
- [11] V Girault. Curl-conforming finite element methods for Navier-Stokes equations with non-standard boundary conditions in \mathbb{R}^3 . In *The Navier-Stokes Equations Theory and Numerical Methods*, pages 201–218. Springer, 1990.
- [12] Ralf Hiptmair. Finite elements in computational electromagnetism. *Acta Numerica*, 11(July 2003):237–339, July 2002.
- [13] Qingguo Hong, Jonathan W Siegel, and Jinchao Xu. A priori analysis of stable neural network solutions to numerical pdes. *arXiv preprint arXiv:2104.02903*, 2021.

- [14] Kaibo Hu, Young-Ju Lee, and Jinchao Xu. Helicity-conservative finite element discretization for incompressible mhd systems. *Journal of Computational Physics*, 436:110284, 2021.
- [15] Michael Kraus and Omar Maj. Variational integrators for ideal magnetohydrodynamics. *arXiv preprint arXiv:1707.03227*, 2017.
- [16] Aditi Krishnapriyan, Amir Gholami, Shandian Zhe, Robert Kirby, and Michael W Mahoney. Characterizing possible failure modes in physics-informed neural networks. *Advances in Neural Information Processing Systems*, 34, 2021.
- [17] Horace Lamb. *Hydrodynamics*. Cambridge university press, 1932.
- [18] William J Layton, Carolina C Manica, Monika Neda, and Leo G Rebholz. Helicity and energy conservation and dissipation in approximate deconvolution LES models of turbulence. *Advances and Applications in Fluid Mechanics*, 4(1):1–46, 2008.
- [19] Zongyi Li, Nikola Kovachki, Kamyar Azizzadenesheli, Burigede Liu, Kaushik Bhattacharya, Andrew Stuart, and Anima Anandkumar. Fourier neural operator for parametric partial differential equations. *arXiv preprint arXiv:2010.08895*, 2020.
- [20] Jian-Guo Liu and Wei-Cheng Wang. Energy and helicity preserving schemes for hydro-and magnetohydro-dynamics flows with symmetry. *Journal of Computational Physics*, 200(1):8–33, 2004.
- [21] Zichao Long, Yiping Lu, Xianzhong Ma, and Bin Dong. Pde-net: Learning pdes from data. In *International Conference on Machine Learning*, pages 3208–3216. PMLR, 2018.
- [22] H Keith Moffatt. Helicity and singular structures in fluid dynamics. *Proceedings of the National Academy of Sciences*, 111(10):3663–3670, 2014.
- [23] HK Moffatt. Some developments in the theory of turbulence. *Journal of Fluid Mechanics*, 106:27–47, 1981.
- [24] HK Moffatt and A Tsinober. Helicity in laminar and turbulent flow. *Annual review of fluid mechanics*, 24(1):281–312, 1992.
- [25] Maxim Olshanskii and Leo G Rebholz. Note on helicity balance of the Galerkin method for the 3D Navier-Stokes equations. *Computer Methods in Applied Mechanics and Engineering*, 199(17-20):1032–1035, 2010.
- [26] Jean Carlos Perez and Stanislav Boldyrev. Role of cross-helicity in magnetohydrodynamic turbulence. *Physical review letters*, 102(2):025003, 2009.
- [27] Maziar Raissi, Paris Perdikaris, and George E Karniadakis. Physics-informed neural networks: A deep learning framework for solving forward and inverse problems involving non-linear partial differential equations. *Journal of Computational physics*, 378:686–707, 2019.
- [28] Leo G Rebholz. An energy-and helicity-conserving finite element scheme for the Navier-Stokes equations. *SIAM Journal on Numerical Analysis*, 45(4):1622–1638, 2007.